OPEN ACCESS

KING'S College LONDON

King's Research Portal

DOI:
10.1016/j.devcel.2012.11.003

Document Version
Peer reviewed version

Link to publication record in King's Research Portal

Citation for published version (APA):
Stan, R. V., Tse, D., Deharvengt, S. J., Smits, N. C., Xu, Y., Luciano, M. R., McGarry, C. L., Buitendijk, M., Nemani, K. V., Elgueta, R., Kobayashi, T., Shipman, S. L., Moodie, K. L., Daghlian, C. P., Ernst, P. A., Lee, H-K., Suriawinata, A. A., Schned, A. R., Longnecker, D. S., ... Carrière, C. (2012). The diaphragms of fenestrated endothelia: gatekeepers of vascular permeability and blood composition. *Developmental Cell*, *23*(6), 1203-18. https://doi.org/10.1016/j.devcel.2012.11.003

Citing this paper
Please note that where the full-text provided on King's Research Portal is the Author Accepted Manuscript or Post-Print version this may differ from the final Published version. If citing, it is advised that you check and use the publisher's definitive version for pagination, volume/issue, and date of publication details. And where the final published version is provided on the Research Portal, if citing you are again advised to check the publisher's website for any subsequent corrections.

General rights
Copyright and moral rights for the publications made accessible in the Research Portal are retained by the authors and/or other copyright owners and it is a condition of accessing publications that users recognize and abide by the legal requirements associated with these rights.

•Users may download and print one copy of any publication from the Research Portal for the purpose of private study or research.
•You may not further distribute the material or use it for any profit-making activity or commercial gain
•You may freely distribute the URL identifying the publication in the Research Portal

Take down policy
If you believe that this document breaches copyright please contact librarypure@kcl.ac.uk providing details, and we will remove access to the work immediately and investigate your claim.

Download date: 05. May. 2023

NIH Public Access
Author Manuscript
Dev Cell. Author manuscript; available in PMC 2013 December 11.

Published in final edited form as:
Dev Cell. 2012 December 11; 23(6): 1203–1218. doi:10.1016/j.devcel.2012.11.003.

The diaphragms of fenestrated endothelia – gatekeepers of vascular permeability and blood composition

Radu V. Stan[1,2,6,7,*], **Dan Tse**[1], **Sophie J. Deharvengt**[1], **Nicole C. Smits**[3,6], **Yan Xu**[1], **Marcus R. Luciano**[1], **Caitlin L. McGarry**[1], **Maarten Buitendijk**[2], **Krishnamurthy V. Nemani**[5], **Raul Elgueta**[2], **Takashi Kobayashi**[3,6], **Samantha L. Shipman**[3,6], **Karen L. Moodie**[3,6], **Charles P. Daghlian**[1], **Patricia A. Ernst**[2,4], **Hong-Kee Lee**[1], **Arief A. Suriawinata**[1], **Alan R. Schned**[1], **Daniel S. Longnecker**[1], **Steven N. Fiering**[2,4], **Randolph J. Noelle**[2], **Barjor Gimi**[5], **Nicholas W. Shworak**[3,6], and **Catherine Carrière**[3,7]

[1]Department of Pathology, Geisel School of Medicine at Dartmouth, Hanover, NH, USA

[2]Department of Microbiology and Immunology, Geisel School of Medicine at Dartmouth, Hanover, NH, USA

[3]Department of Medicine, Geisel School of Medicine at Dartmouth, Hanover, NH, USA

[4]Department of Genetics, Geisel School of Medicine at Dartmouth, Hanover, NH, USA

[5]Department of Radiology, Geisel School of Medicine at Dartmouth, Hanover, NH, USA

[6]Heart and Vascular Research Center, Geisel School of Medicine at Dartmouth, Hanover, NH, USA

[7]Norris Cotton Cancer Center, Geisel School of Medicine at Dartmouth, Hanover, NH, USA

SUMMARY

Fenestral and stomatal diaphragms are endothelial subcellular structures of unknown function that form on organelles implicated in vascular permeability: fenestrae, transendothelial channels and caveolae. PV1 protein is required for diaphragm formation *in vitro*. Here, we report that deletion of the PV1-encoding *Plvap* gene in mice results in the absence of diaphragms and decreased survival. Loss of diaphragms did not affect the fenestrae and transendothelial channels formation but disrupted the barrier function of fenestrated capillaries causing a major leak of plasma proteins. This disruption results in early death of animals due to severe non-inflammatory protein loosing enteropathy. Deletion of PV1 in endothelium, but not the hematopoietic compartment, recapitulates the phenotype of global PV1 deletion, whereas endothelial reconstitution of PV1 rescues the phenotype. Taken together, these data provide genetic evidence for the critical role of the diaphragms in fenestrated capillaries in the maintenance of blood composition.

© 2012 Elsevier Inc. All rights reserved.

*Contact: Radu V. Stan, M.D., Department of Pathology, The Geisel School of Medicine at Dartmouth, 1 Medical Center Drive, Lebanon, NH 03756. Tel: (603) 650-8781, Fax: (603) 650-6120, Radu.V.Stan@Dartmouth.edu.

Contributions: RVS, DT, SJD, NCS, YX, MRL, CLM, MB, KVN, RE, TK, SLS, KLM, and CC performed experiments. HKL, ARS, AAS and DSL evaluated pathology specimens. PE provided critical reagents. RVS, DT, SNF, RJN, CPD, BG and CC designed experiments. RVS, NWS and CC wrote the paper.

Online supplemental material
For more experimental details, see Supplementary Methods.

Publisher's Disclaimer: This is a PDF file of an unedited manuscript that has been accepted for publication. As a service to our customers we are providing this early version of the manuscript. The manuscript will undergo copyediting, typesetting, and review of the resulting proof before it is published in its final citable form. Please note that during the production process errors may be discovered which could affect the content, and all legal disclaimers that apply to the journal pertain.

$watermark-text
$watermark-text
$watermark-text

$watermark-text

$watermark-text

$watermark-text

INTRODUCTION

Microvascular permeability is a vital function by which endothelial cells (ECs) in combination with their glycocalyx and basement membranes from capillaries and postcapillary venules (the so-called exchange segment of the vascular tree), control the exchange of molecules between the blood plasma and the interstitial fluid, while maintaining blood and tissue homeostasis (Bates, 2010; Dvorak, 2010; Komarova and Malik, 2010; Levick and Michel, 2010). A clear understanding of the molecular mechanisms involved in the control of microvascular permeability continues to elude us, fueling persisting controversy as to which pathways are employed by different molecules in order to cross the endothelial barrier (Predescu et al., 2007; Rippe et al., 2002). To cross the EC monolayer proper, molecules use either a paracellular (*i.e.* in between the cells) or a transcellular (*i.e.* across the cells) route. Transcellular exchange is accomplished via either solute transporters, or transcytosis via vesicular carriers (*e.g.* caveolae), or pore-like subcellular structures (*i.e.* fenestrae and transendothelial channels (TECs)) [reviewed in (Aird, 2007; Tse and Stan, 2010).

A large part of the problem is the lack of understanding of the function of the different endothelial subcellular structures involved in permeability, adopted by ECs in the exchange segment of different vascular beds (Aird, 2007; Tse and Stan, 2010). Among these structures are caveolae, fenestrae and TECs. Fenestrae are 60–80nm diameter transcellular pores spanned by fenestral diaphragms (FDs), except in the ECs of kidney glomerulus and the liver sinusoids (Clementi and Palade, 1969a; Reeves et al., 1980; Wisse, 1970). FDs consist of radial fibrils (Bearer and Orci, 1985) and display tufts of heparan sulfate proteoglycans on their luminal side (Simionescu et al., 1981). TECs thought to be fenestrae precursors, occur interspersed with fenestrae in attenuated areas of the ECs albeit at approximately 5–20 fold lower surface density, depending on the vascular bed (Milici et al., 1985). TECs are spanned by two diaphragms without heparan sulfate proteoglycan tufts (Rostgaard and Qvortrup, 1997). Caveolae are plasma membrane invaginations, which in ECs of select vascular beds (*i.e.* lung and all fenestrated ECs) display a thin protein barrier-like structure in their necks called a stomatal diaphragm (SD) (Stan et al., 1999a).

FDs occur at sites where molecules are adsorbed from the interstitium into the blood stream (i.e. endocrine glands, kidney peritubular capillaries and intestine villi). Tracer experiments (Clementi and Palade, 1969a) as well as whole organ studies (Levick and Smaje, 1987) have suggested that FDs and the “glycocalyx tufts” present on their luminal side, form a combined filter acting as a permselective barrier allowing the passage of water and small molecules (i.e. ions, sugars, amino acids, small peptide hormones) and blocking the extravasation of macromolecules [reviewed in (Levick and Michel, 2010)]. While information exists on the molecular diameter cut-off of the basement membrane, opinions vary as to the contribution of proteoglycans and diaphragm to the filter (Bearer and Orci, 1985; Levick and Smaje, 1987). Tracer studies also hint to a barrier function for SDs in caveolae (Clementi and Palade, 1969a; Villaschi et al., 1986) but the physiological implications are still unclear. There is little knowledge on the precise function of TECs.

The removal of a long-standing obstacle in studying the function of endothelial diaphragms was initiated by proteomic studies identifying a homodimeric endothelial membrane glycoprotein, namely PV1, as the first known molecular component of both FDs and SDs (Stan, 2004; Stan et al., 1999a; Stan et al., 1999b; Stan et al., 1997). PV1 is necessary to form FDs and SDs in cells in culture (Ioannidou et al., 2006; Stan et al., 2004). Moreover, formation of FDs and SDs appears to be the sole cellular function of PV1 in ECs (Tkachenko et al., 2012). Recently, the deletion of PV1 in mice was reported confirming the role of PV1 in forming both FDs and SDs *in vivo* (Herrnberger et al., 2012a; Herrnberger et

$watermark-text

$watermark-text

$watermark-text

al., 2012b). A model by which the FDs and SDs are similar structures consisting of a framework of radial fibrils made of PV1 homodimers was proposed (Tse and Stan, 2010). However, this model is not a matter of general consensus, other studies disputing the role of PV1 in diaphragm formation (Hnasko and Ben-Jonathan, 2005; Hnasko et al., 2006a).

With the exception of two reports (Hnasko et al., 2006b; Hnasko et al., 2002), most data agree on PV1 being an endothelial specific protein [reviewed in (Tse and Stan, 2010)]. This is also supported by PV1 being the antigen of two classic "anti-endothelial" monoclonal antibodies MECA-32 (Hallmann et al., 1995) and PAL-E (Niemela et al., 2005) and studies of LacZ knock-in in Plvap locus in mice (Herrnberger et al., 2012a; Herrnberger et al., 2012b). PV1 has emerging roles in cancer (Carson-Walter et al., 2005; Deharvengt et al., 2012; Madden et al., 2004), diapedesis of leukocytes in sites of inflammation (Keuschnigg et al., 2009), inflammatory (Mozer et al., 2010) and ocular disease (Chen et al., 2012; Paes et al., 2011; Schafer et al., 2009).

Herein, we exploit the obligate role of PV1 in diaphragm formation to examine *in vivo* the role of FDs in the maintenance of permselectivity in fenestrated endothelia and thereby in blood plasma composition. Using independently generated mice with loss and gain of PV1 function, we also confirm that endothelial PV1 is required for diaphragm formation *in vivo*, and that the diaphragms in organs with fenestrated vessels are essential for maintaining endothelial barrier function, basal permeability and blood composition. Impairment of FD function in PV1 deficient mice leads to selective loss of plasma proteins with consequent edema and dyslipidemia, gradually resulting in multiple organ dysfunction. PV1 deficient mice succumb to a lethal, non-inflammatory, protein loosing enteropathy. Thus, PV1 mediated endothelial barrier function is critical for mammalian survival.

RESULTS

PV1 is essential for intrauterine and postnatal survival

To determine the function of PV1 protein and endothelial diaphragms *in vivo*, mice were generated that carried *LoxP* sites inserted into introns 1 and 5 of the mouse *PV1/Plvap* locus ($PV1^{L/L}$ mice)(Fig. 1A, S1A). By breeding the $PV1^{L/L}$ mice with *CMV-cre* mice, which express the cre recombinase under the control of the ubiquitously activated cytomegalovirus-derived promoter (CMV), we generated $PV1^{-/-}$ mice, lacking PV1 in all tissues (Fig. 1A, S1B–C). PV1 absence following disruption of the *PV1/Plvap* gene was confirmed at mRNA (Fig. 1B) and protein level (Fig. 1C).

Homozygous disruption of the *PV1/Plvap* gene led to sharply decreased survival that varied depending on the mouse strain used. On pure C57Bl/6J background, PV1 deletion resulted in 100% lethality between embryonic day E13 (embryonic day 13) and P2 (postnatal day 2). On hybrid intercrosses containing a mix of Balb/c (50%), C57Bl/6J (37.5%) and 129Sv/J (12.5%) backgrounds, ~20% of the expected frequency of homozygous $PV1^{-/-}$ mice survived up to 3–4 months of age (Fig. 1D–E). The heterozygote $PV1^{+/-}$ had decreased PV1 mRNA (Fig. 1B) and protein levels (Fig. 5B), but did not exhibit any obvious phenotype on either C57BL/6J or mixed backgrounds. All the subsequent experiments in $PV1^{-/-}$ mice were carried out on mixed Balb/c - C57Bl/6J - 129Sv/J background because it was the only one that allowed the study of postnatal $PV1^{-/-}$ phenotype.

At birth, $PV1^{-/-}$ mice displayed normal appearance and normal size but gradually developed signs of growth retardation and wasting. Decreased average body weight was significant in both genders by P4 progressing in severity as the mice aged (Fig. S1D). At 4 week-old $PV1^{-/-}$ mice had ~30–40% reduction in body weight (Fig. S1D) and ~15% in body length (Fig. S1E–F). The small body size was accompanied by a generalized decrease in white

$watermark-text

$watermark-text

$watermark-text

adipose tissue deposits in the abdominal wall, retroperitoneal and gonadal fat pads as shown by MRI in 3–4 week-old live $PV1^{-/-}$ mice (Fig. S1G) and a reduced gonadal fat pad/body weight ratio postmortem (Fig. S1H). By that age *PV1*$^{-/-}$ mice also developed a distended abdomen due to accumulation of ascites (not shown). Aside from an abnormally bent tail observed in ~70% of mutant mice (Fig. S1E), no defect in organ appearance and size (as determined by organ/body weight ratio, data not shown) were observed at birth in *PV1*$^{-/-}$ mice. Past 1 week of age, $PV1^{-/-}$ pancreata displayed an abnormally reduced size as evidenced by pancreas/body weight ratio (Fig. S1I). All organs, including the pancreas had normal histological appearance (Fig. S2A).

PV1 is essential for the formation of endothelial diaphragms *in situ*

In vitro studies have shown that PV1 is required for diaphragm formation (Ioannidou et al., 2006; Stan et al., 2004) suggesting that PV1 loss *in vivo* would prevent diaphragm formation in fenestrae, TECs and caveolae. To confirm this critical finding, we conducted morphometric analyses in adult *PV1*$^{-/-}$ mice of mixed background using both transmission and scanning electron microscopy. Diaphragm presence was determined by a combination of ultrathin sectioning (20–40nm), specimen tilting and morphometry. We examined 1) organs with fenestrated capillaries where caveolae, TEC and fenestrae exhibit diaphragms (i.e. adrenals, choroid plexus, kidney, pituitary, thyroid, intestinal villi, salivary glands and pancreas), 2) the continuous endothelium of lung capillaries that exhibits only caveolae with SDs, and 3) the two organs with fenestrated endothelia where PV-1 and diaphragms are normally absent (kidney glomerular and liver sinusoidal capillaries).

Caveolae diaphragms were also absent in $PV1^{-/-}$ capillaries from lung (Fig. 1G), adrenals (Fig. 1H), pancreas (Fig. 1I), pituitary, thyroid, kidney, intestinal villi, and liver (not shown), as compared to WT exemplified for the lung (Fig. 1F). In lungs, the surface density of EC caveolae (not shown) and the protein levels of its structural component caveolin 1 (Fig. 1C) were unchanged in *PV1*$^{-/-}$ mice by comparison to WT and $PV1^{+/-}$ mice (not shown). The levels of VE Cadherin were also similar (Fig. 1C) suggesting a similar number of vessels.

In control mice, diaphragms were observed in fenestrae and TECs of all fenestrated capillaries examined, as exemplified by kidney peritubular capillaries (Fig. 1J). Such diaphragms were absent in the corresponding $PV1^{-/-}$ capillaries (Table 1). Instead, only open conduits/pores in the size range of fenestrae and TECs (~50–120 nm), lacking any electron opaque structure indicative of the diaphragms, were found. Figure 1 illustrates the findings in *PV1*$^{-/-}$ capillaries from adrenals (Fig. 1H), pancreas (Fig. 1I), intestine (Fig. S2Ba), choroid plexus (Fig. S2Bb), pituitary (Fig. S2Bc), thyroid (Fig. S2Bd), and kidney peritubular capillaries (Fig. 1J,K and S2Be). Without diaphragms, it was not possible to reliably discriminate if these pores were fenestrae or TECs. However, the $PV1^{-/-}$ pore surface density (3.87 +/−0.54 stdev) was comparable to the aggregated fenestrae/TEC density in wild type (WT)(4.11 +/− 0.36 stdev) peritubular capillaries of kidney (Fig. 1L). Of minor note, fenestral pores in *PV1*$^{-/-}$ mice exhibited a larger variation of diameter (Fig. 1L, right panel).

In kidney glomerular and liver sinusoidal capillaries, mature fenestrae without FDs are developmentally preceded by PV1-positive fenestrae with FDs (Bankston and Pino, 1980; Ichimura et al., 2008; Wisse, 1970). As demonstrated by the normal fenestrae morphology in sinusoidal (Fig. 1M,N) and glomerular (Fig. 1O–Q) ECs in *PV1*$^{-/-}$ mice when compared to WT, PV1 is not involved, even transiently, in the formation of mature fenestrae in these vascular segments.

In conclusion, PV1 is necessary for the *in vivo* formation of diaphragms but is not required for the formation of caveolae or of fenestrae/TEC pores.

$watermark-text

$watermark-text

$watermark-text

Endothelial specific loss of PV1 phenocopies PV1 germline deletion

To define PV1 functions in ECs and evaluate potential roles in non-endothelial cell types, we generated PV1 cell-type specific knockout mice and compared them to $PV1^{-/-}$ animals. $PV1^{L/L}$ mice were bred with *Tie2-cre* and *VEC-cre* transgenic mouse lines, generating $PV1^{ECKO\text{-}Tie2}$ and $PV1^{ECKO\text{-}VEC}$ mice, respectively (Fig. 2A, Table 2), that target both endothelial and hematopoietic cell compartments during embryogenesis. To discriminate between the impacts of PV1 absence in the endothelial compartment versus hematopoietic compartment, $PV1^{L/L}$ mice were also crossed with *Vav1-cre* mice (Stadtfeld and Graf, 2005), which express cre exclusively in the hematopoietic compartment ($PV1^{HCKO\text{-}Vav}$) (Fig. 2A, Table 2).

$PV1^{ECKO\text{-}Tie2}$ and $PV1^{ECKO\text{-}VEC}$ exhibited a PV1 deletion efficiency >95% (Fig. S2A) and ~70–90% (not shown), respectively, consistent with previous reports (Chen et al., 2009). $PV1^{HCKO\text{-}Vav}$ mice exhibited ~100% deletion in the hematopoietic cells in blood, skin (tail), peritoneal lavage and spleen (Fig. S2B). Deletion in the tail (Fig. S2B) was negligible, consistent with the hematopoietic lineage specific activity of the Vav1 promoter. At the protein level, PV1 levels were drastically reduced in the lungs of $PV1^{ECKO\text{-}Tie2}$ (Fig. 2B) and $PV1^{ECKO\text{-}VEC}$ (not shown) mice, while normal in $PV1^{HCKO\text{-}Vav}$ (Fig. 2C), as compared to littermate controls.

The deletion of *PV1/Pvlap* in endothelial and hematopoietic cells lineages in both $PV1^{ECKO\text{-}Tie2}$ and $PV1^{ECKO\text{-}VEC}$ mice fully phenocopied $PV1^{-/-}$ mice with respect to survival: on pure C57Bl/6J background there were no survivors after P2, while on hybrid C57Bl/6J;129Sv/J (87.5%;12.5%) backgrounds, ~20–30% of the expected frequency of each mouse line survived to 3–4 ($PV1^{ECKO\text{-}Tie2}$) or 6–7 ($PV1^{ECKO\text{-}VEC}$) months (Fig. 2D–E, Table 2). In contrast, no mortality was observed in $PV1^{HCKO\text{-}Vav}$ mice (Fig. 2D–E). As observed in $PV1^{-/-}$ mice, $PV1^{ECKO\text{-}VEC}$ and $PV1^{ECKO\text{-}Tie2}$ but not $PV1^{HCKO\text{-}Vav}$ mice displayed growth retardation (Fig. S2C) with normal organ morphology and histology, reduced pancreas size and white fat tissue deposits and ascites formation (not shown).

As observed in $PV1^{-/-}$ mice, both $PV1^{ECKO\text{-}Tie2}$ and $PV1^{ECKO\text{-}VEC}$ mice lacked diaphragms in endothelial fenestrae, TECs and caveolae in pancreas (Fig. 2Fa,i), intestine (Fig. 2Fb), kidney (Fig. 2Fc,e–g), lung (Fig. 2Fd) and adrenals (Fig. 2Fh,j) whereas, diaphragms were not affected in the $PV1^{HCKO\text{-}Vav}$ mice (Fig. 2Fl). These data were confirmed by formal morphometric analysis that was carried out only in kidneys and lungs of $PV1^{ECKO\text{-}Tie2}$ mice (Table 1). $PV1^{ECKO\text{-}Tie2}$ liver fenestrae morphology (Fig. 2Fk) was indistinguishable from WT (Fig. 1M).

Therefore, PV1 expression in the endothelium but not hematopoietic cells is essential for mouse survival and the cellular and gross phenotype observed in $PV1^{-/-}$ mice stems from loss of PV1 in ECs.

Loss of endothelial PV1 and diaphragms results in disrupted blood composition

The absence of diaphragms should result in leakage of all plasma components with molecular diameters between 6–30nm, representing the interval between the upper pore sizes determined for fenestrated capillaries and their basement membranes respectively (Sarin, 2010). This would encompass all plasma proteins except those that occur in extremely large complexes or lipoprotein particles. Conversely, plasma electrolytes should be relatively unaffected.

Indeed $PV1^{-/-}$ mice, versus control littermates, showed a sharp decrease in total plasma protein, albumin and albumin/globulin ratio (Fig. 3A–C) associated with minimal electrolyte imbalance featuring a lower calcium concentration (TableS1). Hypoproteinemia developed

progressively postnatally with plasma protein levels of $PV1^{-/-}$ mice, compared to control WT and $PV1^{+/-}$ littermates, minimally lower at birth (not shown), 30–40% reduced after one week, 50–70% reduced after 4 weeks, and continuing to fall with age (Fig. 3A–C). The altered plasma composition was clearly due to PV1 loss in ECs, as both $PV1^{ECKO\text{-}Tie2}$ (Fig. 3D) and $PV1^{ECKO\text{-}VEC}$ (not shown) mice exhibited similar levels of hypoproteinemia, whereas $PV1^{HCKO\text{-}Vav}$ mice showed no changes in plasma protein levels (not shown).

SDS-protein acrylamide gel electrophoresis of plasma showed that hypoproteinemia in $PV1^{-/-}$ and $PV1^{ECKO\text{-}Tie2}$ mice affected most classes of serum proteins except for proteins larger than 200kD, which did not decrease with age (Fig. 3E). Similarly, serum protein agarose gel electrophoresis showed that plasma from $PV1^{-/-}$, $PV1^{ECKO\text{-}Tie2}$, and $PV1^{ECKO\text{-}VEC}$ mice had relative decreases in albumin and β globulin fractions, and a large relative increase in the α globulin fractions (Fig. 3F), also demonstrated by densitometry (Fig. S3A). The α globulin fractions include some of the largest circulating proteins such as α2 macroglobulin (950kD), haptoglobin, pentameric IgM (900kD), ceruloplasmin (135kD) and ApoB apolipoproteins (250kD and 500kD), also suggesting that mostly lower molecular weight proteins contribute to hypoproteinemia. A prominent loss of smaller proteins was clearly demonstrated by analysis of protein composition of the ascites fluid formed in both $PV1^{-/-}$ and $PV1^{ECKO}$ mice, which contained albumin and β globulins at the same level with blood plasma but had sharply diminished α fractions (Fig. 3F). Combined, these data suggest that PV1 endothelial deficiency leads to “sieving hypoproteinemia”, characteristic of hypoproteinemia due to protein loss (*i.e.* protein losing enteropathy or nephropathy), in which “smaller” plasma proteins preferentially disappear from the plasma.

Major blood plasma proteins are produced in the liver, except for the immunoglobulins (Ig), which are produced by immune cells. Absolute plasma levels of IgA (Fig. 3G), IgM (Fig. 3H) and IgG (not shown) were reduced in 4 week-old $PV1^{-/-}$ as compared to WT and $PV1^{+/-}$ littermates. Thus, hypoproteinemia affected levels of proteins produced both in the liver and the immune system.

Other possible causes of hypoproteinemia include decreased production (*i.e.* due to liver dysfunction, malnutrition or amino acid malabsorption), increased catabolism or protein loss (due to protein losing enteropathy or nephropathy). The Ig reduction was not due to an intrinsic defect in plasma cells, as isolated $PV1^{-/-}$ plasma cells were perfectly able to produce Ig *in vitro*, as determined by ELISPOT (not shown). To determine whether liver function was impaired, we carried out liver function tests of plasma (*e.g.* plasma liver enzymes, bilirubin, IgA). $PV1^{-/-}$ and $PV1^{ECKO}$ mice and their control littermates exhibited similar liver enzymes (AST, ALT, ALP; when standardized to total protein), bilirubin (both direct and indirect) levels (TableS1) and low IgA levels (Fig. 3G). Liver production of mRNAs for major plasma proteins (albumin, transferrin, fibrinogen) was found to be higher in $PV1^{-/-}$ mice (Fig. S3B). These results argue against impaired liver function in $PV1^{-/-}$ mice. We were also able to exclude food intake and malabsorption due to pancreatic dysfunction as causes of hypoproteinemia (R.V. Stan unpublished data).

Although the observed sieving effect in plasma protein composition suggested the possibility of a nephropathy, $PV1^{-/-}$ and $PV1^{ECKO}$ mice at different ages exhibited normal kidney histology (Fig. S2A and S3D) and unaltered glomerular ultrastructure (Fig. 1O,Q). No protein was found in the urine of $PV1^{-/-}$ mice between birth and 12 weeks of age. Blood urea nitrogen (Fig. S3C) and creatinine levels (TableS1), as well as urinalysis tests on random or 24h urine were also normal. Thus, endothelial loss of PV1 does not impair kidney function and does not enhance protein catabolism.

$watermark-text $watermark-text $watermark-text

$watermark-text

$watermark-text

$watermark-text

Based on published literature, the gradual decrease in plasma protein should be followed by a certain degree of hypertriglyceridemia due to decreased lipoprotein lipase activity in peripheral tissues and decreased consumption of dietary triglyceride-rich lipoprotein particles such as chylomicron remnants (Shearer and Kaysen, 2006; Yoshino et al., 1993). Moreover, because the particle size of >200nm is much larger than fenestrae/TEC pores, chylomicron apolipoproteins such as ApoB48 should be spared from plasma protein loss exhibited by $PV1^{-/-}$ mice, further demonstrating the sieving. Consistent with these predictions, plasma lipids were normal in postnatal $PV1^{-/-}$ mice up to 2 weeks of age (not shown) - a period of time during which hypoproteinemia first developed. Past 2 weeks, $PV1^{-/-}$ plasma showed marked lipid accumulation as shown by its milky aspect (Fig. 3I) and by electron microscopy (Fig. 3J). The severity of lipid accumulation gradually increased with age, initially confined to the plasma by 4 weeks of age (Fig. 3J, left), accompanied by xanthoma (lipid-containing white deposits) on the surface of the heart and liver after 8 weeks (Fig. S3E) and later (10–12 weeks) perivascular lipid deposits were formed (Fig. 3J, right); post 8 weeks in several tissues lipids were seen engorging the capillaries (Fig. 3J, middle; S3F).

Consistent with these observations, direct lipid measurements in lithium heparin plasma or in serum from $PV1^{-/-}$ and control littermates at 4 weeks of age showed severe (10–30 fold) increase in plasma triglycerides (TG) (1500–2000mg/dL) and moderately increased total cholesterol (CHOL) (175–250mg/dL) with significantly decreased HDL cholesterol fraction (HDLc) (20–60mg/dL) in $PV1^{-/-}$ mice (TableS1). Plasma TG levels further increased 30–100 fold (up to 5000–6000mg/dL) from 4 to 8 week-old (Fig. 3K–L) both in $PV1^{-/-}$ and $PV1^{ECKO}$ mice followed by a slower gradual increase until death at 12–14 weeks (not shown). In contrast, the elevated total CHOL and reduced HDLc fractions detected in $PV1^{-/-}$ and $PV1^{ECKO}$ plasma did not vary considerably with time (Fig. 3K–L). Only extended (24 hours) fasting led to a slow plasma TG level decrease to around 300mg/dL (Fig. 3M), suggesting that slow TG hydrolysis from the lipoprotein particles is one of the probable causes of hypertriglyceridemia. Fasting did not affect CHOL or HDLc levels (Fig. 3M). $PV1^{HCKO}$ and $PV1^{+/-}$ mice had normal lipid levels (Fig. 3I, TableS1).

TGs normally occur in chylomicrons, chylomicrons remnants (CMR) and very low-density lipoproteins (VLDL). $PV1^{-/-}$ mice exhibited a dramatic increase in CMR/VLDL as revealed by TEM analysis of the lumen of blood vessels (Fig. 3I) and by gel filtration FPLC of plasma samples, showing that CMRs/VLDLs contained the bulk of TG and CHOL (Fig. 3N). This identification was further supported by increased ApoB apolipoproteins in the plasma and FPLC fractions (Fig. 3N,P). There was a dramatic increase of ApoB48 lipoprotein over the ApoB100 (Fig. 3O,P) suggesting a dietary/intestinal origin for these particles. The intestine is able to produce chylomicrons (Fig. S3F). Liver overproduction of VLDL seemed unlikely, based on ApoB and fatty acid synthase mRNA levels being normal (Fig. S3G).

Combined these data demonstrate that diaphragm deletion leads to sieving hypoproteinemia, hypertriglyceridemia and increased plasma concentration of chylomicron remnants.

Lack of endothelial PV1 compromises endothelial barrier function to proteins in fenestrated vessels

At 3–4 weeks, $PV1^{-/-}$ organs provided with fenestrated vessels (*e.g.* intestine, kidney and pancreas) showed signs of edema, while heart, liver, brain and spleen did not show significant changes (Fig. 4A), as assessed by wet/dry organ weight ratio. Histologically, intestinal villi were distended with protein-containing material accumulating between the enterocytes and stroma (Fig. 4B). ECs did not surround this material, which persisted even after 24h starvation and did not stain with lipid probes such as Oil RedO (not shown), ruling

$watermark-text

$watermark-text

$watermark-text

out the possibility that these spaces were lipid-containing distended lymphatics/lacteals. The absence of an inflammatory infiltrate in the intestine (Fig. 4B) and any other organs (Fig. S2A) showed that edema was not a consequence of inflammation. Altogether, these results strongly suggest that the absence of diaphragms in *PV1*$^{-/-}$ mice produces a leaky fenestrated endothelium.

Plasma proteins leakage into the interstitial space was also examined using the Evans Blue (EB) dye extravasation assay (Bates, 2010). EB binds tightly to plasma proteins (especially albumin) and is normally retained in the vascular space, its extravasation demonstrating protein leakage into the interstitial space. *PV1*$^{-/-}$ mice being severely hypoproteinemic, EB was pre-bound to purified mouse serum albumin before administration and tissues were harvested after 5 and 15 minutes, when there is very little EB-albumin extravasation in WT organs. EB-albumin extravasation was dramatically increased at 15min in *PV1*$^{-/-}$ and *PV1*^{ECKO} organs with fenestrated ECs (*e.g.* intestine, pancreas and kidney), in 4 (Fig. 4C), and 8 (Fig. 4D) week old mice. Consistent with histological findings, the intestine displayed the highest rate of EB leakage out of its capillaries (Fig. 4C–E). Minimal increase in EB extravasation was observed in the *PV1*$^{-/-}$ lungs (continuous endothelium expressing PV1 and SDs)(Fig. 4C, right) or heart (continuous endothelium lacking PV1/diaphragms) (Fig. 4C–D) but no change was detected in the liver (fenestrated endothelium without FDs but expressing PV1 in SDs) (Fig. 4C–D).

EB-albumin extravasation was detected in the ascites in 4 week old *PV1*$^{-/-}$ mice (Fig. 4F). Moreover, EB-albumin was also detected in the lumen of *PV1*$^{-/-}$ small intestine (Fig. 4F), clearly demonstrating protein loss through the intestinal mucosa. Similar results were observed in *PV1*$^{ECKO\text{-}Tie2}$ mice (not shown).

Next, we used fluorescent tracers of various sizes to evaluate the upper pore size (*i.e.* the diameter of the molecules that do not gain passage across the endothelium) of the fenestrated capillaries in absence of diaphragms. Fluorescent mouse albumin (average molecular radius of 3.6nm), IgG_2(5.5nm), IgM(12nm), and dextrans of 10KD (~2.3nm) and 70KD (5.77nm) average molecular weight were readily detected in the ascites at 5 and 15 min post administration, whereas dextran with an average size of 2×10^6D (~27.9nm) leaked much slower (Fig. 4G). To corroborate these findings at EM level we introduced in the circulation of *PV1*$^{-/-}$ mice albumin coated gold nanoparticles of 10, 15 and 25nm and the site of leakage determined at 5min of tracer perfusion. We found that, in *PV1*$^{-/-}$ mice, albumin-gold particles of all these sizes are able to exit adrenal capillaries, and the gold particles were clearly associated with diaphragm-less fenestrae/TEC (Fig. 4Ha–e). These data show an increased pore size for *PV1*$^{-/-}$ fenestrated capillaries and identify fenestrae as sites of leakage.

Combined, these data demonstrate that endothelial PV1 is required for maintenance of basal permeability in the adult mouse, particularly in vascular beds with fenestrated capillaries provided with FDs.

Endothelial reconstitution of PV1 rescues the *PV1*$^{-/-}$ phenotype and restores the diaphragms of fenestrae and caveolae

To demonstrate that the *PV1*$^{-/-}$ phenotype is not due to perturbation of other genes near the *PV1/Pvlap* locus, we performed transgenic complementation in which PV1 was reconstituted specifically in ECs of *PV1*$^{-/-}$ mice.

Having previously shown that a HA-tagged PV1 protein behaves as its native counterpart in cultured cells (Stan et al., 2004), we generated mouse lines (*VEC-PV1HA*) expressing PV1-HA under the control of the VE Cadherin promoter and 5′ intronic enhancer (Hisatsune et

$watermark-text

$watermark-text

$watermark-text

al., 2005) (Fig. 5A). From six founder lines, we selected a line expressing PV1HA in all organs (Fig. S4A–B) at ~30–50% of the native PV1 levels in tissues where it is normally expressed such as the lung (Fig. 5B). In 4 week-old mice, PV1-HA was detected in ECs of all vessels, large arteries and veins, capillaries in the heart and muscle, brain vessels and glomerulus and less in the sinusoids of the liver (Fig. S4A–B and not shown). Mosaicism of transgene expression was detected by confocal microscopy (Fig. S5A) and 14.6 (+/− 10.3)% of CD31 or VEC (CD144) positive lung ECs did not express PV1-HA by flow cytometry (not shown). In 4 weeks old mice, PV1-HA was detected in ECs of all vessels, large arteries and veins, capillaries in the heart and muscle, brain vessels and glomerulus and less in the sinusoids of the liver (Fig. S4A–B and not shown). *VEC-PV1HA*$^{+/tg}$ mice did not exhibit any overt phenotype in terms of survival, fertility, growth, blood composition or cardiovascular function.

VEC-PV1HA$^{+/tg}$;PV1$^{-/-}$(*PV1*^{ECRC}) mice were generated (Fig. 5A) and displayed ~30–50% reconstitution of PV1HA (Fig. 5B) when normalized to the lung endothelial content, as measured by VE cadherin levels, an accepted endothelial marker in the adult (Salomon et al., 1992). These subnative levels of PV1 reconstitution significantly increased *PV1*^{ECRC} mice survival to ~60% of expected Mendelian frequency, on a mixed background (Fig. 5C). Moreover, 100% of the *PV1*^{ECRC} mice that survived to 28 days were alive up to 1 year later (Fig. 5D).

Importantly, *PV1*^{ECRC} mice displayed diaphragm restoration in the lung, adrenal, kidney, pancreas, thyroid and intestine (Fig. 5E, Table 1). Consistent with the idea of the mosaicism and hypomorphic PV1 expression (Fig. S4A), in kidney peritubular capillaries, there were isolated ECs that did not form diaphragms or express PV1 (Fig. S4D). Less than 5% of glomerular capillaries exhibiting fenestrae with diaphragms, and no caveolae diaphragms were detected in the heart (Fig. 5Eh), muscle or aorta ECs (not shown).

PV1^{ECRC} mice had normal growth (Fig. 5F), near normal level of plasma proteins (Fig. 5G) CHOL and TGs (Fig. 5H) and no edema in organs with fenestrated endothelia (Fig. S4C). Thus, re-expression of PV1 in ECs of *PV1*$^{-/-}$ mice restores diaphragm formation and rescues their complex vascular leak syndrome.

Discussion

Here, we demonstrated *in vivo* the essential role of PV1 in the formation of FDs and SDs on endothelial organelles such as fenestrae, TEC and caveolae, whereas the lack of expression of PV1 does not affect the formation of these organelles. Most importantly, by enabling the formation of the diaphragms of fenestrae/TEC, PV1 plays a critical role in regulating basal permeability to proteins and the maintenance of blood composition. Removal of the diaphragms resulted in early death of mice caused by severe, non-inflammatory protein losing enteropathy. Thus, the role of PV1-containing diaphragms in regulation of basal permeability is absolutely essential for postnatal survival.

At the ultrastructural/subcellular level, we show that the deletion of PV1 results in complete absence of SDs and FDs *in situ*, confirming previous *in vitro* data (Ioannidou et al., 2006; Stan et al., 2004) and further validating our model by which PV1 is necessary for diaphragm formation. Notwithstanding the inherent technical difficulties in ascertaining the loss of diaphragms by electron microscopy (depending on the thickness of the section and on how much of the fenestrae/TEC pore rim was encompassed in the section), we did not find a single diaphragm in any of the structures we were able to examine in *PV1*$^{-/-}$ and *PV1*$^{ECKO\text{-}Tie2}$ mice. The hypomorphic rescue of PV1 in ECs restores all types of diaphragms and TEC. Interestingly, expression of PV1 *in vivo* restores diaphragms only in

$watermark-text

$watermark-text

$watermark-text

the ECs where they natively occur, demonstrating the essential but not sufficient role PV1 in the diaphragms formation.

PV1 is not necessary for the formation of fenestrae/TEC pores and caveolae. Surface density of these organelles is similar in *PV1*$^{-/-}$ and WT littermates. The only observed difference is in a greater variation in the diameter of fenestrae and TEC in *PV1*$^{-/-}$ mice. These findings are in agreement with the idea generated decades ago that a possible function of diaphragms was to maintain the size, shape and distribution of the fenestrae (Clementi and Palade, 1969b), recently bolstered by *in vitro* studies (Ioannidou et al., 2006). No conduits resembling TEC without diaphragms were found, suggesting either that PV1 is required for TEC pore formation or, more likely, that TEC are precursors of fenestrae and the double diaphragms are required for maintenance of the channel length.

Formation of the diaphragms regulates basal permeability to proteins. Deletion of FDs causes leakage of plasma proteins into the peritoneal cavity and into the interstitium of organs provided with fenestrated capillaries (*i.e.* intestine, kidney, pancreas) but not in organs with continuous endothelium (heart, muscle, lung) in *PV1*$^{-/-}$ and *PV1*^{ECKO} mice. In contrast, the sites where fenestrae have no FDs (*i.e.* liver sinusoids or glomerulus) do not exhibit changes in permeability. The leakage involves most plasma proteins, up to the size of IgM (mol radius 12nm), or tracers as large as 2×10^{6}KD dextran (mol radius 27.9nm), but not the components of the largest lipoprotein particles such as VLDL/chylomicron remnants. We demonstrate that nanoparticles as large as 25nm are able to exit fenestrated vessels on a very fast time scale (5min). Although the EM micrographs do not allow dynamic visualization of the site of leakage, the gold particles (especially the larger ones) were found closely associated with clusters of fenestrae/TEC pores, thus bolstering our claims that in absence of diaphragms fenestrae/TEC pores leak plasma molecules with much larger diameter that in WT.

Thus, the FDs act as size selective molecular sieves with a function reminiscent of that of the podocyte slit diaphragms in the mature kidney glomerulus, which have been more intensively studied. While the molecular architecture is not precisely the same (*i.e.* spoke and wheel radial vs. zipper-like parallel fibrils), both types of diaphragms make use of transmembrane N-linked glycoproteins with large extracellular domains (*i.e.* PV1 and nephrin) revealing a general building principle of vascular sieves. While additional proteins (e.g. Neph-1, FAT1) enable the formation of slit diaphragms, the FD structure might involve other proteins in addition to PV1, which we are actively pursuing.

Lack of caveolar SDs in fenestrated endothelia does not seem to have a role in plasma protein extravasation seen in *PV1*$^{-/-}$ mice, as no differences in EB extravasation are observed between the lungs of *PV1*$^{-/-}$ mice and control, where capillaries contain only caveolar SDs. The lack of role of caveolar SDs in basal permeability is also suggested by the fact that permeability to proteins in continuous endothelia where caveolae do (*i.e.* lung) or do not (*i.e.* heart, skeletal muscle) have SDs is similar [reviewed in (Sarin, 2010)], or it is enhanced when the SDs are present (King et al., 2004). How much of the increased permeability to proteins in *PV1*$^{-/-}$ mice is the result of the deletion of diaphragms of fenestrae or those of TEC and whether knocking out PV1 deletes the proteoglycans within fenestrae, is a matter of further study.

Lack of diaphragms resulted in defects in blood composition and protein losing enteropathy causing early death of *PV1*$^{-/-}$ mice on mixed background. *PV1*$^{-/-}$ and *PV1*^{ECKO} (but not *PV1*^{HCKO}) mice have numerous homeostatic defects, which are rescued by the reconstitution of the diaphragms in ECs of *PV1*^{ECRC} mice, an important confirmation that the defects are directly related to the loss of diaphragms. These defects include significant

$watermark-text

$watermark-text

$watermark-text

growth retardation, declining plasma protein levels, increase in TG-rich lipoprotein particles, edema and ascites formation, consistent with protein calorie malnutrition. The hypoproteinemia is central to the PV1$^{-/-}$ phenotype. While decreased protein production, enhanced protein catabolism and protein loss by nephrotic syndrome were ruled out, intestinal loss of protein as a cause of hypoproteinemia was confirmed by permeability studies in *PV1*$^{-/-}$ and *PV1*^{ECKO} mice, which demonstrated sharply increased protein extravasation and loss in the intestinal lumen.

The increases in TG-rich lipoprotein particles in *PV1*$^{-/-}$ mice follow hypoproteinemia, the former being a known sequel of hypoproteinemia in both humans and rodents (Shearer and Kaysen, 2006; Yoshino et al., 1993). However, the severity of plasma TG increases in *PV1*$^{-/-}$ mice is unusually high and might reflect the magnitude of the protein loss in *PV1*$^{-/-}$ mice or additional mechanisms by which PV1 regulates TG metabolism. The increase in plasma concentration of ApoB48-containing CMRs with diameters much larger than the diaphragm-less fenestrae pores brings strong support to the idea of an increase in the upper pore size of the capillary wall of the PV1$^{-/-}$ fenestrated vessels. Conversely, the leakage is restricted to probes smaller than the fenestrae pores.

In the light of the gradual character of the changes in *PV1*$^{-/-}$ and *PV1*^{ECKO} mice on the mixed 129Sv/J × C57BL/6J background, a plausible scenario unfolds by which the deletion of FDs initially cause extravasation of proteins and moderate hypoproteinemia due to the increase in the volume of the compartment to which plasma proteins have access. This volume now includes the intravascular space and the volume of the interstitial space of the organs with fenestrated vessels. Here, the presence of excess protein will cause gradual edema further increasing the protein compartment volume, which may accentuate hypoproteinemia. It is not clear what is the effect of the plasma protein extravasation and edema on the function of most organs with fenestrated vessels. Future experiments using innovative inducible, vascular bed endothelial specific deletion of PV1 might be able to answer this question. What is clear is that PV1 deletion in mice on mixed background results in an important intestinal edema, which may constitute the basis of the demonstrated intestinal barrier failure and intestinal protein loss. The latter provides a rational explanation for the severe hypoproteinemia and the clear signs of protein calorie malnutrition syndrome resembling kwashiorkor in humans (e.g. growth retardation, severe hypoproteinemia, ascites, hypertriglyceridemia and lipid deposits), which may be the cause of death in PV1$^{-/-}$ mice.

PV1$^{-/-}$ and *PV1*^{ECKO} (but nor *PV1*^{HCKO}) mice exhibited reduced survival with varying severity depending on the background, with the 129/SvJ background mitigating the effects and allowing postnatal life. In all *PV1*$^{-/-}$ and *PV1*^{ECKO} mice examined PV1 and the diaphragms were completely absent; thus the difference in survival was not due to incomplete penetrance of the diaphragm-free phenotype. It is possible that differences in the severity of leakage (in rate and/or components), or the impact of the leakage on the function of critical organs (e.g. circumventricular organs and endocrine glands), or effects of PV1 outside fenestrae, might explain the differences between backgrounds. Further studies in mice with conditional time-resolved deletion/reconstitution of PV1 should elucidate these issues.

While our paper was under review, two papers from the same group were published describing the PV1$^{-/-}$ phenotype in mice generated by a targeted trap insertion in intron 1 of Plvap locus (Herrnberger et al., 2012a; Herrnberger et al., 2012b). In agreement with our data, Herrnberger et al confirm that PV1 is essential for diaphragm formation in caveolae, fenestrae and TEC and is not required for the formation of fenestrae pores themselves. These lend considerable support to our premise that PV1$^{-/-}$ mice constitute a good model for

$watermark-text

$watermark-text

$watermark-text

studying the role of diaphragms in permeability, to which they also agree. Herrnberger et al also observe mouse background-dependent decreased survival, small pancreata and cutaneous hemorrhages in mice that die *in utero (*which we do not show in this paper) in $PV1^{-/-}$ mice. Interestingly, while we do not observe any statistically relevant changes in surface density of fenestral pores in kidney or qualitative changes in pancreas, Herrnberger et al. report a reduction in fenestrae pore numbers in kidney and pancreas although no formal quantification was performed. Another difference, related to the first, is that they did not detect pancreatic edema, which they assessed by qualitative morphology only. These data lead them to speculate that PV1 knockout mouse could have reduced permeability. In contrast, our measurements demonstrate pancreatic, intestinal, kidney and skin edema with dramatically increased permeability in organs with fenestrated vessels.

These differences could be explained in part by the different mouse genetic backgrounds used in both studies, as we both clearly demonstrated the impact of the background on phenotype severity. The different designs for the null allele (trap insertion in intron 1 and LacZ expression vs. deletion of exons 2–5) could also be contributing factors. These differences should inform future studies of PV1 function such as ruling out dominant negative effects of truncation PV1 mutants or the effects of exogenous protein expression.

In summary, deletion of PV1 protein *in vivo* allowed us to demonstrate that the diaphragms of fenestrae and TEC are critical for the maintenance of endothelial barrier integrity and basal permeability. In the absence of such diaphragms, plasma protein extravasation produces a non-inflammatory protein losing enteropathy resulting in protein calorie malnutrition and ultimately death. Our results and the unique mouse models we have created provide the foundations for evaluating numerous aspects of basal permeability in fenestrated vascular beds.

Experimental Procedures

Mice

Generation of the $PV1^{L/L}$ mice—The PV1loxP targeting vector loxP recombination sites in intron 1 and 5, schematized in Fig. 1A, was constructed by Bacterial Artificial Chromosome recombination technology. $PV1^{L/L}$ mice were generated by knock-in using homologous recombination in mice (Fig. S1C–D) at Dartmouth Transgenics Facility.

Targeted PV1 deletion—$PV1^{L/L}$ mice were bred to *CMV-cre*, *Tie2-cre*, *VEC-cre* and *Vav-cre* mice, to delete exons 2–5 of the *Plvap* locus in the germline, endothelial and hematopoietic or hematopoietic only compartments. Genotypes generated are detailed in Table 2.

Generation of VEC-PV1HA transgenic mice—The VEC-PV1HA transgenic cassette consisting of the VEC promoter, mouse PV1 fused to 3xHA epitope, SV40 polyA signal sequence and the 5′ 5kb of the VE Cadherin intron 1 was used for transgenic mouse generation at Dartmouth Transgenic Facility. $VEC\text{-}PV1HA^{+/-}$ lines were characterized in terms of PV1 expression pattern in blood vessels.

PV1HA reconstitution in $PV1^{-/-}$ mice—$VEC\text{-}PV1HA^{+/-}$ mice were bred to $PV1^{+/-}$ to obtain $VEC\text{-}PV1HA^{+/-};PV1^{+/-}$ mice, which were further bred to $PV1^{+/-}$ to obtain $PV1HA^{+/-}$;$PV1^{-/-}$ ($PV1^{ECRC}$) mice.

Survival analysis—The survival rate of different mouse genotypes mice was calculated from the total observed numbers in each mouse line and assuming a Mendelian distribution

$watermark-text

$watermark-text

$watermark-text

of genotypes according to the breeding scheme employed. The statistical significance was calculated using the CHI^2 test.

Transmission electron microscopy and morphometry—Organs were harvested and processed for routine transmission electron microscopy, as described (Tkachenko et al., 2012). Briefly, mice were euthanized with CO_2, and their vasculature immediately flushed free of blood by 5 min perfusion via the left ventricle using the left atrium as an outlet (also ensuring the perfusion of lung vasculature) of HBSS containing calcium and magnesium (HBSS-CM) followed by 10min of EM fixative (2% glutaraldehyde, 3% paraformaldehyde, 0.1M sodium cacodylate, pH7.2). Tissues were harvested, cut in 1×2mm blocks and fixed further in fresh fixative, rinsed in 0.1M sodium cacodylate, postfixed in 1% OsO_4 in 0.1M sodium cacodylate, briefly rinsed, stained en block with Kellenberger's uranyl acetate in water, dehydrated through graded ethanol and embedded in LX-112 resin (Ladd Research) using propylene oxide for ethanol substitution. Ultrathin sections of 20–40nm were cut using an ultrasonic diamond knife (Diatome) mounted on grids, stained with uranyl acetate and lead citrate and examined in a Jeol 1010 electron microscope using a bottom mount AMD camera.

For morphometry, pictures of 75 random capillaries (*i.e.* vessels with <10μm diameter) were taken from three animals per group (2–5 blocks/animal, 4 animals/genotype) at a magnification of 5,000X. The number of the caveolae, fenestrae and TEC were expressed as a function of membrane length examined (at least 10μm in each section). The number of fenestrae/TEC pores per μm linear length of membrane was determined by the method of Milici, et al (Milici et al., 1985; Tkachenko et al., 2012). Student's *t* test was used to determine statistical significance between different groups.

Scanning electron microscopy—Organs were harvested and fixed as above, osmicated, dehydrated in graded ethanol, freeze-fractured in liquid nitrogen and transferred back in 100% ethanol from where they were subjected to critical point dying using a Samdri 795 device (tousimis). Dried tissue blocks were mounted on carbon tape coated 12mm stubs, osmium coated using an OPC-60N Osmium Plasma Coater Model (SPI) and examined under XL-30 ESEM-FEG field emission gun environmental scanning electron microscope (FEI) operated at 15kV. Images were collected at 10,000–20,000x magnification.

mRNA isolation and real time quantitative PCR—Tissues were collected in RNAlater (Qiagen) and total RNA isolated using Trizol (Sigma). RNA integrity and purity were determined using Bioanalyzer (Agilent) and NanoDrop (Thermo-Fisher). RNA was reverse transcribed and amplified for quantitative real-time PCR using Taqman® Gene Expression Assays (Applied Biosystems). A list of the Gene Expression Assays used is in Supplemental Methods. The comparative C_T method ($2^{-\Delta\Delta CT}$) of relative quantitation was used to compare different genotypes.

Isolation of mouse lung total membranes and blotting

Lung membrane lysates were obtained as described (Stan et al., 1999a). Proteins were separated by SDS- polyacrylamide gel electrophoresis and either silver stained or transferred to PVDF membranes and immunoblotted with various antibodies.

Isolation of cells for genotyping or flow cytometry—Mouse tissues were flushed free of blood, organs were excised, collagenase treated, a single cell suspension prepared and labeled with antibodies as described in Supplemental Methods.

$watermark-text

$watermark-text

$watermark-text

Isolation of blood plasma—Mice were euthanized, their thoracic cavity opened and blood collected from the heart on heparin Microtainer tubes (BD Bioscience). The samples were centrifuged at 6000xg for 15 min to obtain platelet-poor plasma.

Isolation of hematopoietic cells—Blood was harvested in EDTA-coated Microtainer tubes (BD Biosciences), centrifuged to pellet the blood cells, red blood cells were lysed, white blood cells were collected by centrifugation and used for genomic DNA isolation. Peritoneal cells were harvested by peritoneal lavage using PBS/2% serum albumin/5mM EDTA and were profiled to determine content of CD45-expressing cells, usually >95%. Spleens were dissociated by mechanical disruption through a 70μm mesh, yielding <5% non-hematopoietic cells.

Blood plasma measurements (comprehensive metabolic panels, lipid profiles, albumin and total protein) were done on a chemistry analyzer (Roche MODULAR PPE) by the Dartmouth Department of Pathology Clinical Chemistry Laboratory. Protein subclass determination was done on serum on a Hydrasys-LC system (Sebia). QuantiChrome™ kits for total protein, albumin, CHOL and TGs determination were used, as per manufacturer's instructions (BioAssay Systems). Random or fasting venous blood was collected with a heparin coated capillary tube, and spotted on the strips of an Accu-Check Instant Plus device (Roche) as per manufacturer's instructions.

Serum IgG, IgM and IgA levels were determined using ELISA kits (ICL), as per manufacturer's instructions.

Plasma lipoprotein fractionation was done by FPLC (Superose 6, GE Healthcare) at a flow rate of 0.25 ml/min, and 0.5-ml fractions were collected.

Magnetic Resonance Imaging and Fat Volume Determination were performed on a 7T Varian Unity Inova magnetic resonance spectrometer equipped with a triple axes gradients, as described in Supplemental Methods.

Organ/Body weight ratio—Organs were removed, weighed, dried in an oven at 80°C for 7 days, weighed again and wet/dry weight ratio was calculated.

Histology—Mouse organs were fixed in 10% buffered formalin and embedded in paraffin. For Oil RedO fat content analysis, organs were fixed (24h, RT) in methanol-free 4% paraformaldehyde in PBS, followed by cryoembedding in OCT (Tissue-Tek).

Evans Blue dye extravasation assay—Under anesthesia with isofluorane, mice were injected i.v. with 100μl/20g body weight of sterile 2% Evans Blue, 6% mouse serum albumin (99.9% pure, MP Bio) in 0.9 % saline. To determine Evans Blue extravasation in the organs, the tracer was allowed to circulate for the noted amount of time, when the mice were euthanized and their vasculature perfused (1ml/min, 10 min, RT) with PBS via the left and right ventricles to remove the intraluminal dye from the systemic and pulmonary circulation, respectively. Organs of interest were harvested, weighed, extracted in formamide and Evans Blue content calculated as detailed in Supplemental Methods. The Evans Blue content in the peritoneal cavity and intestinal lumen was determined at 5 and 15min without PBS perfusion ensuring minimal disruption to the circulation.

Leakage of tracers directly labeled with fluorophores—Under anesthesia with isofluorane, *PV1*$^{-/-}$ mice were injected i.v. with 100μl/10g body weight of sterile fluorescent tracer in 0.9% saline. The tracers used were bovine serum albumin–Alexa647 (250μM), mouse IgG–Alexa555 (100μM), mouse IgM–Alexa647 and FITC-dextrans with

molecular averages of 10KD, 70KD and 2×10^6D. At the indicated time points, mice were euthanized, ascites fluid collected in *PV1*$^{-/-}$ mice and its fluorescence intensity was determined.

Leakage of albumin-gold nanoparticles—Gold nanoparticles of 10, 15 and 25nm average diameter (EMS) were separately stabilized by coating with bovine serum albumin per manufacturer's instructions, collected by ultracentrifugation, mixed to yield a triple tracer mixture which was adjusted to 1% bovine serum albumin in 0.9 % saline. *PV1*$^{-/-}$ and WT mice (n=4/group, 4 week old) were euthanized and their blood was flushed out by perfusion with PBS via the left ventricle, while ligatures were placed on the abdominal aorta above and below the renal arteries and the abdominal aorta was cannulated using a custom made catheter. The kidneys and adrenals were perfused (0.5 ml/min, 5min, RT) with triple tracer preparation via abdominal aorta using a nick in the inferior vena cava as an outlet, followed by removal of excess gold particles by perfusion of PBS (0.5 ml/min, 5min at RT) and EM fixative perfusion (0.5 ml/min, 10min at RT). Kidneys and adrenals were collected, trimmed into blocks and processed for LX112 embedding and sectioning, as described above. Ultrathin sections were stained with only uranyl acetate to facilitate gold particle detection.

Morphometric analysis of gold nanoparticle extravasation was carried out on EM micrographs of capillaries (i.e. vessels with diameters of less than 10μm) from 3 mice per genotype. For each capillary profile, the number of gold particles of each size found outside the vessel lumen was determined and expressed as particles per micrometer of membrane length.

Statistical significance was determined by two tailed Student's *t* test, analysis of variance (ANOVA), or CHI^2 test, as appropriate.

Supplementary Material

Refer to Web version on PubMed Central for supplementary material.

Acknowledgments

This work was supported from NIH grants HL83249, HL092085, RR16437 (PI Green) and GSM funds to RVS. We thank J. Chen (UNC Chapel Hill) for help with the Plvap targeting construct, N. Speck and M. Chen for VEC-cre, S. Graff for Vav1-cre mice, R. Milne for ApoB antibodies, F. Polito and M. Curtis for plasma measurements and D. Madden and E. Tkachenko for critically reading the manuscript.

Abbreviations

CHOL	cholesterol
EC	endothelial cell
FD	fenestral diaphragm
HDL	high-density lipoproteins
HSPG	heparan sulfate proteoglycan
LDL	low-density lipoproteins
SA	serum albumin
SD	stomatal diaphragm
TEC	transendothelial channel

$watermark-text
$watermark-text
$watermark-text

TG	triglycerides
VLDL	very low density lipoprotein
WT	wild type

References

Aird WC. Phenotypic heterogeneity of the endothelium: I. Structure, function, and mechanisms. Circ Res. 2007; 100:158–173. [PubMed: 17272818]

Bates DO. Vascular endothelial growth factors and vascular permeability. Cardiovasc Res. 2010; 87:262–271. [PubMed: 20400620]

Bearer EL, Orci L. Endothelial fenestral diaphragms: a quick-freeze, deep-etch study. J Cell Biol. 1985; 100:418–428. [PubMed: 3968170]

Carson-Walter EB, Hampton J, Shue E, Geynisman DM, Pillai PK, Sathanoori R, Madden SL, Hamilton RL, Walter KA. Plasmalemmal vesicle associated protein-1 is a novel marker implicated in brain tumor angiogenesis. Clin Cancer Res. 2005; 11:7643–7650. [PubMed: 16278383]

Chen J, Stahl A, Krah NM, Seaward MR, Joyal JS, Juan AM, Hatton CJ, Aderman CM, Dennison RJ, Willett KL, et al. Retinal expression of Wnt-pathway mediated genes in low-density lipoprotein receptor-related protein 5 (Lrp5) knockout mice. PloS one. 2012; 7:e30203. [PubMed: 22272305]

Chen MJ, Yokomizo T, Zeigler BM, Dzierzak E, Speck NA. Runx1 is required for the endothelial to haematopoietic cell transition but not thereafter. Nature. 2009; 457:887–891. [PubMed: 19129762]

Clementi F, Palade GE. Intestinal capillaries. I. Permeability to peroxidase and ferritin. J Cell Biol. 1969a; 41:33–58. [PubMed: 5775791]

Clementi F, Palade GE. Intestinal capillaries. II. Structural effects ofEDTA and histamine. J Cell Biol. 1969b; 42:706–714. [PubMed: 4979362]

Deharvengt SJ, Tse D, Sideleva O, McGarry C, Gunn JR, Longnecker DS, Carriere C, Stan RV. PV1 downregulation via shRNA inhibits the growth of pancreatic adenocarcinoma xenografts. J Cell Mol Med. 2012

Dvorak HF. Vascular permeability to plasma, plasma proteins, and cells: an update. Curr Opin Hematol. 2010; 17:225–229. [PubMed: 20375889]

Hallmann R, Mayer DN, Berg EL, Broermann R, Butcher EC. Novel mouse endothelial cell surface marker is suppressed during differentiation of the blood brain barrier. Dev Dyn. 1995; 202:325–332. [PubMed: 7626790]

Herrnberger L, Ebner K, Junglas B, Tamm ER. The role of plasmalemmal vesicle-associated protein (PLVAP) in endothelial cells of Schlemm's canal and ocular capillaries. Exp Eye Res. 2012a

Herrnberger L, Seitz R, Kuespert S, Bosl MR, Fuchshofer R, Tamm ER. Lack of endothelial diaphragms in fenestrae and caveolae of mutant Plvap-deficient mice. Histochem Cell Biol. 2012b; 138:709–724. [PubMed: 22782339]

Hisatsune H, Matsumura K, Ogawa M, Uemura A, Kondo N, Yamashita JK, Katsuta H, Nishikawa S, Chiba T. High level of endothelial cell-specific gene expression by a combination of the 5′ flanking region and the 5′ half of the first intron of the VE-cadherin gene. Blood. 2005; 105:4657–4663. [PubMed: 15746076]

Hnasko R, Ben-Jonathan N. Developmental regulation of PV-1 in rat lung: association with the nuclear envelope and limited colocalization with Cav-1. Am J Physiol Lung Cell Mol Physiol. 2005; 288:L275–284. [PubMed: 15640522]

Hnasko R, Carter JM, Medina F, Frank PG, Lisanti MP. PV-1 labels trans-cellular openings in mouse endothelial cells and is negatively regulated by VEGF. Cell Cycle. 2006a; 5:2021–2028. [PubMed: 16969078]

Hnasko R, Frank PG, Ben-Jonathan N, Lisanti MP. PV-1 is negatively regulated by VEGF in the lung of caveolin-1, but not caveolin-2, null mice. Cell Cycle. 2006b; 5:2012–2020. [PubMed: 16969073]

$watermark-text $watermark-text $watermark-text

$watermark-text

$watermark-text

$watermark-text

Hnasko R, McFarland M, Ben-Jonathan N. Distribution and characterization of plasmalemma vesicle protein-1 in rat endocrine glands. J Endocrinol. 2002; 175:649–661. [PubMed: 12475376]

Ichimura K, Stan RV, Kurihara H, Sakai T. Glomerular endothelial cells form diaphragms during development and pathologic conditions. J Am Soc Nephrol. 2008; 19:1463–1471. [PubMed: 18480313]

Ioannidou S, Deinhardt K, Miotla J, Bradley J, Cheung E, Samuelsson S, Ng YS, Shima DT. An in vitro assay reveals a role for the diaphragm protein PV-1 in endothelial fenestra morphogenesis. Proc Natl Acad Sci U S A. 2006; 103:16770–16775. [PubMed: 17075074]

Keuschnigg J, Henttinen T, Auvinen K, Karikoski M, Salmi M, Jalkanen S. The prototype endothelial marker PAL-E is a leukocyte trafficking molecule. Blood. 2009; 114:478–484. [PubMed: 19420356]

King J, Hamil T, Creighton J, Wu S, Bhat P, McDonald F, Stevens T. Structural and functional characteristics of lung macro- and microvascular endothelial cell phenotypes. Microvasc Res. 2004; 67:139–151. [PubMed: 15020205]

Komarova Y, Malik AB. Regulation of endothelial permeability via paracellular and transcellular transport pathways. Annu Rev Physiol. 2010; 72:463–493. [PubMed: 20148685]

Levick JR, Michel CC. Microvascular fluid exchange and the revised Starling principle. Cardiovasc Res. 2010; 87:198–210. [PubMed: 20200043]

Levick JR, Smaje LH. An analysis of the permeability of a fenestra. Microvasc Res. 1987; 33:233–256. [PubMed: 3587078]

Madden SL, Cook BP, Nacht M, Weber WD, Callahan MR, Jiang Y, Dufault MR, Zhang X, Zhang W, Walter-Yohrling J, et al. Vascular gene expression in nonneoplastic and malignant brain. Am J Pathol. 2004; 165:601–608. [PubMed: 15277233]

Milici AJ, L'Hernault N, Palade GE. Surface densities of diaphragmed fenestrae and transendothelial channels in different murine capillary beds. Circ Res. 1985; 56:709–717. [PubMed: 2581719]

Mozer AB, Whittemore SR, Benton RL. Spinal microvascular expression of PV-1 is associated with inflammation, perivascular astrocyte loss, and diminished EC glucose transport potential in acute SCI. Curr Neurovasc Res. 2010; 7:238–250. [PubMed: 20590523]

Niemela H, Elima K, Henttinen T, Irjala H, Salmi M, Jalkanen S. Molecular identification of PAL-E, a widely used endothelial-cell marker. Blood. 2005; 106:3405–3409. [PubMed: 16099878]

Paes KT, Wang E, Henze K, Vogel P, Read R, Suwanichkul A, Kirkpatrick LL, Potter D, Newhouse MM, Rice DS. Frizzled 4 is required for retinal angiogenesis and maintenance of the blood-retina barrier. Invest Ophthalmol Vis Sci. 2011; 52:6452–6461. [PubMed: 21743011]

Predescu SA, Predescu DN, Malik AB. Molecular determinants of endothelial transcytosis and their role in endothelial permeability. Am J Physiol Lung Cell Mol Physiol. 2007; 293:L823–842. [PubMed: 17644753]

Reeves WH, Kanwar YS, Farquhar MG. Assembly of the glomerular filtration surface. Differentiation of anionic sites in glomerular capillaries of newborn rat kidney. J Cell Biol. 1980; 85:735–753. [PubMed: 6156176]

Rippe B, Rosengren BI, Carlsson O, Venturoli D. Transendothelial transport: the vesicle controversy. J Vasc Res. 2002; 39:375–390. [PubMed: 12297701]

Rostgaard J, Qvortrup K. Electron microscopic demonstrations of filamentous molecular sieve plugs in capillary fenestrae. Microvasc Res. 1997; 53:1–13. [PubMed: 9056471]

Salomon D, Ayalon O, Patel-King R, Hynes RO, Geiger B. Extrajunctional distribution of N-cadherin in cultured human endothelial cells. J Cell Sci. 1992; 102(Pt 1):7–17. [PubMed: 1500442]

Sarin H. Physiologic upper limits of pore size of different blood capillary types and another perspective on the dual pore theory of microvascular permeability. J Angiogenes Res. 2010; 2:14. [PubMed: 20701757]

Schafer NF, Luhmann UF, Feil S, Berger W. Differential gene expression in Ndph-knockout mice in retinal development. Invest Ophthalmol Vis Sci. 2009; 50:906–916. [PubMed: 18978344]

Shearer GC, Kaysen GA. Endothelial bound lipoprotein lipase (LpL) depletion in hypoalbuminemia results from decreased endothelial binding, not decreased secretion. Kidney Int. 2006; 70:647–653. [PubMed: 16807550]

Simionescu M, Simionescu N, Silbert JE, Palade GE. Differentiated microdomains on the luminal surface of the capillary endothelium. II. Partial characterization of their anionic sites. J Cell Biol. 1981; 90:614–621. [PubMed: 6457053]

Stadtfeld M, Graf T. Assessing the role of hematopoietic plasticity for endothelial and hepatocyte development by non-invasive lineage tracing. Development. 2005; 132:203–213. [PubMed: 15576407]

Stan RV. Multiple PV1 dimers reside in the same stomatal or fenestral diaphragm. Am J Physiol Heart Circ Physiol. 2004; 286:H1347–1353. [PubMed: 14630628]

Stan RV, Ghitescu L, Jacobson BS, Palade GE. Isolation, cloning, and localization of rat PV-1, a novel endothelial caveolar protein. J Cell Biol. 1999a; 145:1189–1198. [PubMed: 10366592]

Stan RV, Kubitza M, Palade GE. PV-1 is a component of the fenestral and stomatal diaphragms in fenestrated endothelia. Proc Natl Acad Sci U S A. 1999b; 96:13203–13207. [PubMed: 10557298]

Stan RV, Roberts WG, Predescu D, Ihida K, Saucan L, Ghitescu L, Palade GE. Immunoisolation and partial characterization of endothelial plasmalemmal vesicles (caveolae). Mol Biol Cell. 1997; 8:595–605. [PubMed: 9247641]

Stan RV, Tkachenko E, Niesman IR. PV1 is a key structural component for the formation of the stomatal and fenestral diaphragms. Mol Biol Cell. 2004; 15:3615–3630. [PubMed: 15155804]

Tkachenko E, Tse D, Sideleva O, Deharvengt SJ, Luciano MR, Xu Y, McGarry CL, Chidlow J, Pilch PF, Sessa WC, et al. Caveolae, fenestrae and transendothelial channels retain PV1 on the surface of endothelial cells. PloS one. 2012; 7:e32655. [PubMed: 22403691]

Tse D, Stan RV. Morphological heterogeneity of endothelium. Semin Thromb Hemost. 2010; 36:236–245. [PubMed: 20490976]

Villaschi S, Johns L, Cirigliano M, Pietra GG. Binding and uptake of native and glycosylated albumin-gold complexes in perfused rat lungs. Microvasc Res. 1986; 32:190–199. [PubMed: 3762426]

Wisse E. An electron microscopic study of the fenestrated endothelial lining of rat liver sinusoids. J Ultrastruct Res. 1970; 31:125–150. [PubMed: 5442603]

Yoshino G, Hirano T, Nagata K, Maeda E, Naka Y, Murata Y, Kazumi T, Kasuga M. Hypertriglyceridemia in nephrotic rats is due to a clearance defect of plasma triglyceride: overproduction of triglyceride-rich lipoprotein is not an obligatory factor. J Lipid Res. 1993; 34:875–884. [PubMed: 8354953]

$watermark-text

$watermark-text

$watermark-text

HIGHLIGHTS

- PV1 expression in vascular endothelium is required for survival
- PV1 is required for the formation of stomatal and fenestral diaphragms
- Lack of diaphragms in fenestrated endothelia causes vascular leak of plasma proteins
- Vascular leak results in severe hypoproteinemia and hypertriglyceridemia

$watermark-text
$watermark-text
$watermark-text

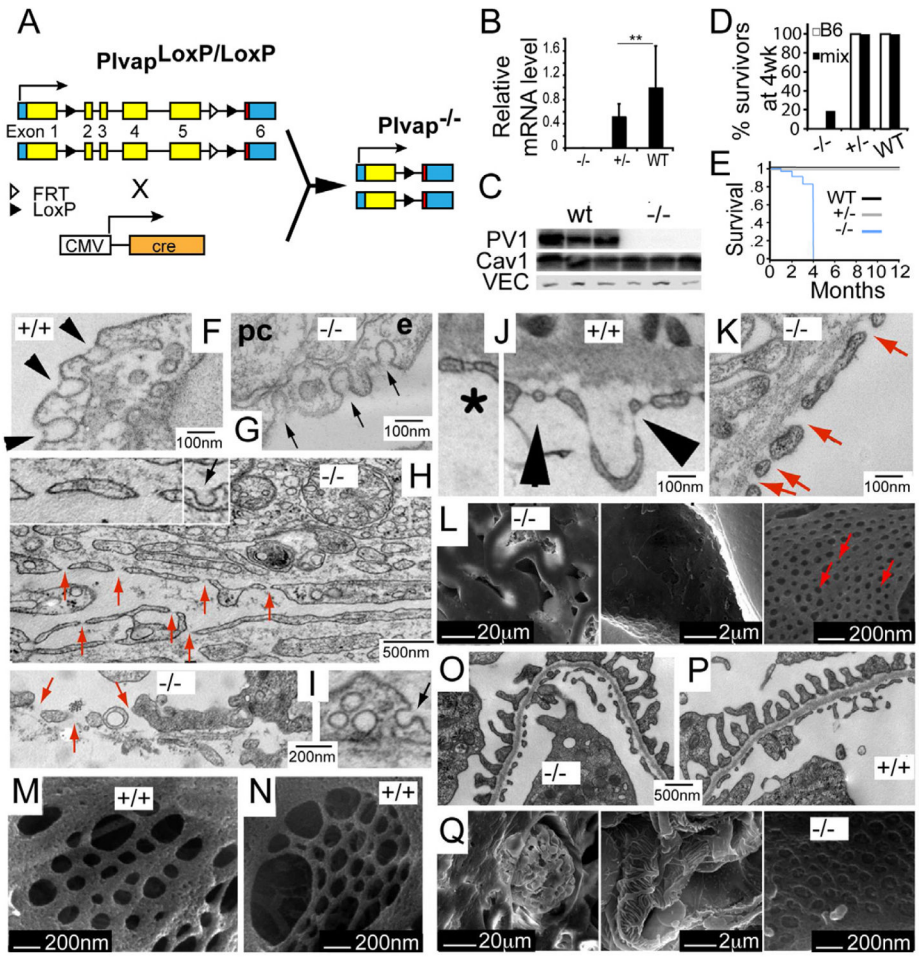

Fig. 1. Lack of PV1 results in absence of endothelial diaphragms and decreased survival

A. Endogenous *Pvlap/PV1* alleles deletion in all cell types via CMV-cre expression.

B. PV1 mRNA levels in the liver of WT, $PV1^{+/-}$ and $PV1^{-/-}$ mice (n>4, stdev, **p <0.01).

C. PV1, Cav1 and VE Cadherin protein levels shown by Western blotting of lung tissue from $PV1^{-/-}$ mice and controls.

D. Mouse survival at 28 days expressed as a percentage of the expected numbers (calculated assuming a mendelian distribution of offspring genotypes) of the indicated genotypes on either C57Bl/6 (white bars) or C57Bl/6-Balb/c-129Sv/J mixed background (solid bars). ($p < 0.01$, CHI^2).

E. Kaplan Mayer analysis of the survival rate of the WT (n=485), $PV1^{+/-}$ (n=899) and $PV1^{-/-}$ (n=92) mice on mixed background that survived past 28 days.

F–Q. Transmission (**F–K,O–P**) and scanning (**L–N, Q**) electron micrographs from tissues of WT (+/+)(**F,J,M,P**) and $PV1^{-/-}$ (−/−)(**G–I,K,L,N,O,Q**) mice. Transmission EM micrographs are from lung (F–**G**), adrenal (**H**), pancreas (**I**), kidney peritubular (**J–K)** and glomerular (**O–P)** ECs. The absence of caveolae SDs (*black arrows)* and of fenestrae FDs (*red arrows*) in $PV1^{-/-}$ mice is indicated. *Black arrowheads* indicate the presence of caveolae SDs (**F**) and of fenestrae FDs (**J**) in WT tissues. The *asterisk* in **J** indicates a TEC with SDs.

Scanning electron micrographs of liver sinusoidal fenestrae sieve plates (**M-N**), or increasing magnification (left to right) of kidney peritubular (**L)** or kidney glomerular (**Q**)

$watermark-text
$watermark-text
$watermark-text

capillaries. The right panels in **O** and **Q** demonstrate diaphragm less fenestrae at high surface density in *PV1*$^{-/-}$ mice.

$watermark-text

$watermark-text

$watermark-text

$watermark-text

$watermark-text

$watermark-text

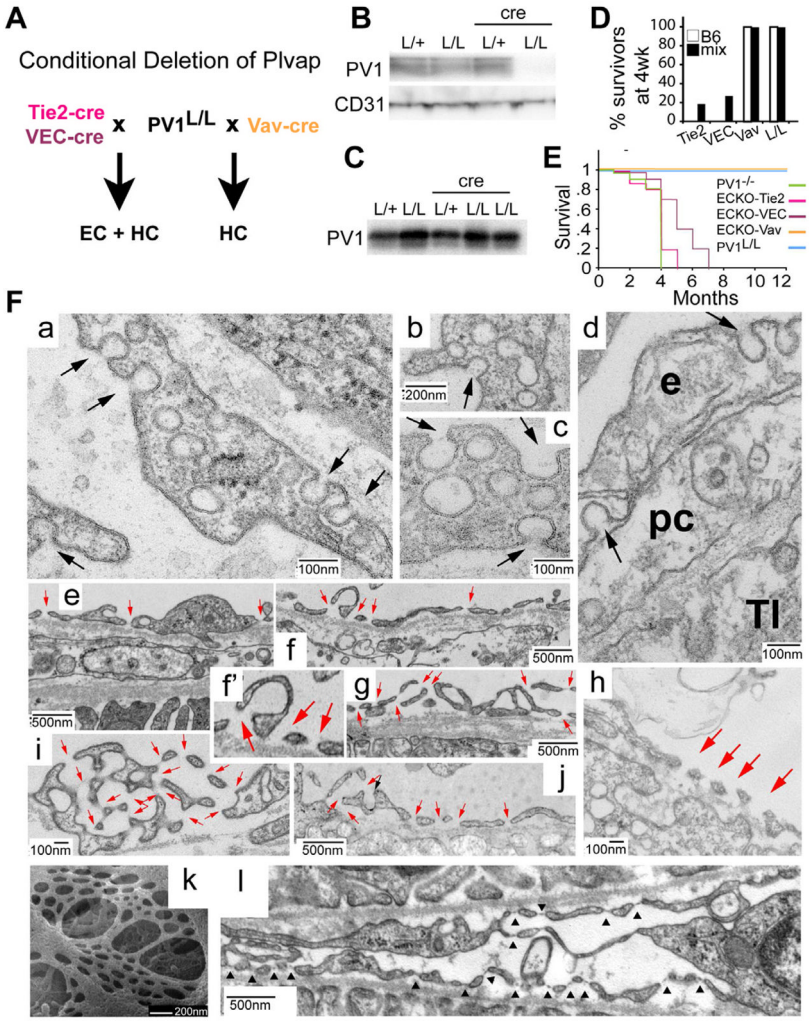

Fig. 2. Deletion of PV1 in endothelial cells but not hematopoietic cells phenocopies the full PV1 knockout

A. Schematic of targeted deletion of *Plvap/PV1* gene in both endothelial and hematopoietic compartments via Tie2-cre and VE Cadherin-cre, and in the hematopoietic compartment only using Vav1-cre. (EC: endothelial cells) and (HC: hematopoietic cells)

B–C. Western blotting of total lung membranes from $PV1^{ECKO\text{-}Tie2}$ (**B**) and $PV1^{HCKO\text{-}Vav}$ mice (**C**) and controls with anti-PV1 antibodies.

D. Mouse survival at 28 days expressed as a percentage of the expected numbers (calculated assuming a mendelian distribution of offspring genotypes) of the indicated genotypes on either C57Bl/6 (white bars) or C57Bl/6- 129Sv/J mixed background (solid bars) ($p < 0.01$, CHI^2).

E. Kaplan-Mayer analysis of the survival rate of $PV1^{L/L}$ (n=274), $PV1^{ECKO\text{-}VEC}$ (n=36), $PV1^{ECKO}$-Tie2 (n=79) and $PV1^{HCKO\text{-}Vav}$ (n=22) on C57Bl/6-129Sv/J mixed background that survived past 28 days. $PV1^{-/-}$ (n=92) mice were also plotted as reference.

F. Electron micrographs demonstrating the absence of diaphragms in $PV1^{ECKO\text{-}Tie2}$ (a,d–f,f′,i–k) and $PV1^{ECKO\text{-}VEC}$ (b–c,g,h) mice (*arrows*) and their presence in the $PV1^{HCKO\text{-}Vav1}$ (l) mice (*arrowheads*). Images are from pancreas (a,i), intestine (b), kidney (c,e–g, l), lung (d), adrenals (h, j), and liver (k). (k, scanning electron micrograph).

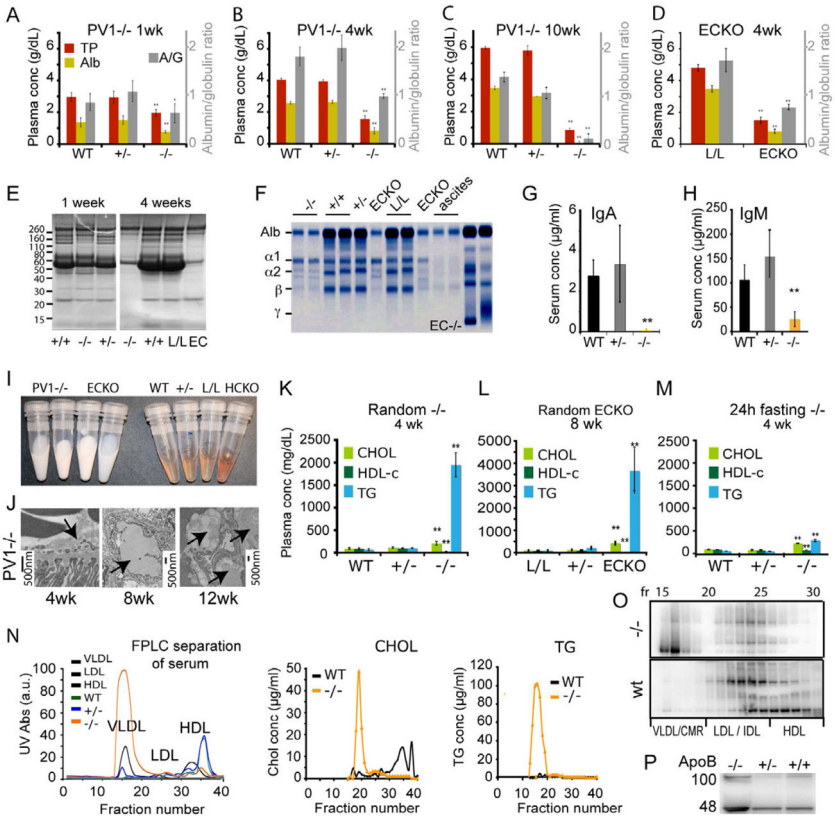

Fig. 3. PV1$^{-/-}$ mice gradually develop a severe hypoproteinemia and hypertriglyceridemia

A–D. Total plasma protein (TP), albumin (Alb) levels and albumin/globulin ratio (A/G) in non-fasted 1 and 4 week-old (A, B), 24h fasted 10 week-old (C) *PV1*$^{-/-}$ mice and 4 week-old *PV1*$^{ECKO\text{-}Tie2}$ mice (D) with control littermates (n>5, *p<0.05, **p<0.01)

E. Coommassie Blue staining of a 7% SDS PAGE of equal volumes (1μl) of blood plasma collected from 1 (left) and 4 (right) week-old PV1$^{-/-}$, PV1$^{ECKO\text{-}Tie2}$ and control mice, as indicated.

F. Equal volumes of serum or ascites fluid from 4 week-old *PV1*$^{-/-}$, WT, *PV1*$^{+/-}$, *PV1*$^{ECKO\text{-}Tie2}$, *PV1*$^{L/+}$, *PV1*$^{L/L}$ and *PV1*$^{ECKO\text{-}VEC}$ mice were subjected to agarose gel protein electrophoresis. Note that the ascites sample came from the *PV1*$^{-/-}$ and *PV1*$^{ECKO\text{-}Tie2}$ mice whose serum is loaded on lanes 1 and 6 from left, respectively. Last two lanes on the right are reference human serum samples.

G–H. Immunoglobulin A (IgA) and M (IgM) plasma levels in 4 week-old *PV1*$^{-/-}$ versus control mice. (n>4–6, **p<0.01)

I. Lithium heparin plasma obtained from *PV1*$^{-/-}$ or *PV1*^{ECKO} mice (left) has a lipid-rich, milky appearance as compared to plasma of WT, *PV1*$^{+/-}$, *PV1*$^{L/L}$ or *PV1*^{HCKO} mice (right).

J. Electron micrographs showing the presence of lipophylic lipid particles (*arrow*) in the plasma of kidney peritubular capillary (left) of a 28 day-old *PV1*$^{-/-}$ mouse. At 8 weeks of age lipids (*asterisk*) in the plasma may coalesce and fully plug capillaries (middle). At 10–12 weeks (right) lipid cuffs (*asterisks*) surround capillaries in many organs.

K–M. Plasma lipid profiles in 4 week-old *PV1*$^{-/-}$ (K), 8 week-old *PV1*$^{ECKO\text{-}Tie2}$ (L) mice and 24 hours fasted 4 week-old *PV1*$^{-/-}$ mice (n>8, for K and n>5 for L,M, *p<0.05, **p<0.01).

N. Size exclusion by fast protein liquid chromatography (FPLC) of serum from *PV1*$^{-/-}$ and control littermates. Left: UV absorption profiles of FPLC fractions from PV1$^{-/-}$ (orange),

$watermark-text
$watermark-text
$watermark-text

PV1$^{+/-}$ (blue) and WT (green) serum. Elution peaks of human VLDL, LDL and HDL controls are also shown (black). Average CHOL (middle) and TG (right) concentration in serum FPLC fractions from *PV1*$^{-/-}$ (orange) and control (black) mice. (FPLC: fast protein liquid chromatography; LDL: low density lipoprotein; VLDL: very low density lipoprotein; HDL: high density lipoprotein)

O–P. Western blotting with an ApoB antibody recognizing both ApoB48 and ApoB100 apolipoproteins of (O) serum FPLC fractions and (P) total plasma samples from *PV1*$^{-/-}$ and control mice.

All error bars: stdev.

$watermark-text

$watermark-text

$watermark-text

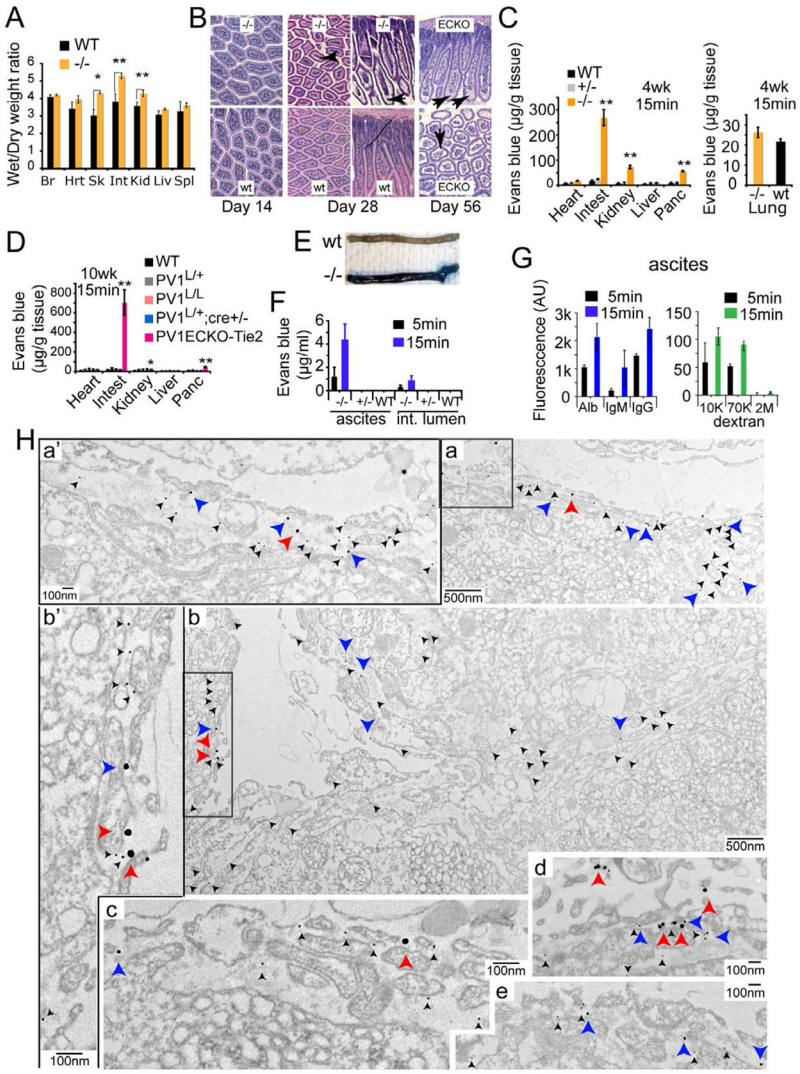

Fig. 4. Vascular leak of proteins in PV1$^{-/-}$ organs provided with fenestrated endothelium

A. Comparison of wet/dry weight ratio of different organs from *PV1*$^{-/-}$ and WT mice at 4 weeks of age.

B. H&E stained sections of formalin fixed paraffin embedded small intestine (jejeunum) of 2 week- (2 left panels), 4 week- (middle 4 panels) and 8 week-old mice (right 2 panels). In the left and middle panels the bottom micrographs demonstrate the intestine from WT (wt) whereas the top micrographs show intestine from *PV1*$^{-/-}$ (−/−) mice. Both micrographs on the right demonstrate the intestine from *PV1*$^{ECKO\text{-}Tie2}$ (ECKO) mice in two different cuts (top - section orthogonal to the intestine wall; bottom - section parallel to the intestinal wall through the intestinal villi). In both *PV1*$^{-/-}$ and *PV1*$^{ECKO\text{-}Tie2}$ samples arrows point to edema.

C–D. Retention of Evans Blue (EB) at 15min following administration of EB-serum albumin in organs of (**C**) 4 week-old *PV1*$^{-/-}$ mice and (**D**) 10 week-old *PV1*$^{ECKO\text{-}Tie2}$ mice and controls (n=4, **p<0.01).

E. Representative image of duodenum of *PV1*$^{-/-}$ (up) and WT (down) mice at 15 min post EB administration.

F. EB quantification in ascites fluid and intestine lumen of *PV1*$^{-/-}$ mice at 5 minutes post EB administration (n=4, **p<0.01).

$watermark-text
$watermark-text
$watermark-text

G. Measurement of leakage of fluorophore-labeled tracers in the ascites fluid of *PV1*$^{-/-}$ mice at 5 and 15min post EB administration (data expressed as arbitrary fluorescence units). (n>3, p<0.01 vs WT)

H a–e. Representative electron micrographs documenting leakage of serum albumin-gold nanoparticles in the adrenals of PV1$^{-/-}$ mice. Arrowheads indicate the position of 10nm (black), 15nm (blue) and 25nm (red) albumin-gold conjugates after 5min perfusion of the tracer mixture. a and b show lower magnification fields with details magnified in a′ and b′. b is a montage of two separate micrographs of adjacent fields. All error bars: stdev.

$watermark-text

$watermark-text

$watermark-text

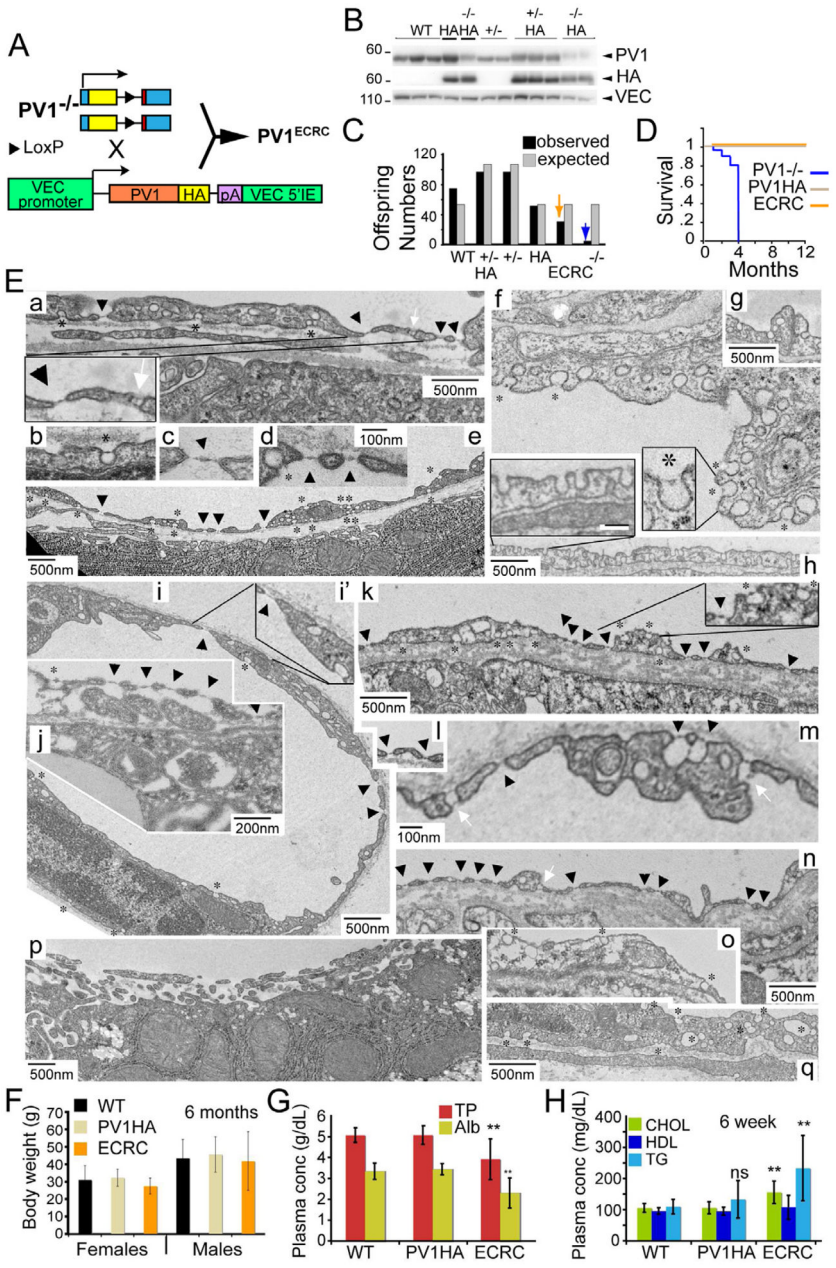

Fig. 5. Endothelial specific reconstitution of PV1 rescues the PV$^{-/-}$ phenotype

A. Schematic of endothelial specific PV1 reconstitution in *PV1^{ECRC}* mice.

B. Western blotting of equal amounts of lung membrane proteins with anti-PV1, anti-HA and anti-VE Cadherin antibodies.

C. Survival of *PV1^{ECRC}* and control genotypes at weaning on a mixed background. The orange and blue arrows highlight the observed differences in of *PV1^{ECRC}* and *PV1$^{-/-}$* offspring numbers, respectively.

D. Kaplan Mayer analysis of the survival of *PV1^{ECRC}*, *PV1HA* and *PV1$^{-/-}$* mice that survived past 4 week-old.

E. Electron micrographs documenting the reconstitution of SDs and FDs in capillary endothelia of *PV1^{ECRC}* mice: kidney (a,a′–c), pancreas (d,e), lung (f,g), heart (h), intestine villus (i, i′), adrenal (j), thyroid (k,l), salivary glands (m), thyroid (n,o) and liver sinusoid (p)

$watermark-text
$watermark-text
$watermark-text

and liver centrolobular vein (q). FDs are indicated with *arrowheads*, SDs of TEC with *white arrows* whereas SCs of caveolae are indicated by *asterisks*. Insets show higher magnification of relevant details.

F–G. Comparison in 6 month-old $PV1^{ECRC}$, *PV1HA* (HA) and WT mice of (F) body weights of the (n>5, stdev), (G) total plasma protein (TP), albumin (Alb) levels and albumin/globulin ratio (A/G) (n=4, **p<0.01).

H. Plasma total cholesterol (CHOL), HDL cholesterol (HDLc) and triglycerides (TG) concentration of 6 week-old $PV1^{ECRC}$ mice. (n=4, **p<0.01). All error bars: stdev.

$watermark-text

$watermark-text

$watermark-text

$watermark-text $watermark-text $watermark-text

Dev Cell. Author manuscript; available in PMC 2013 December 11.

Table 1

Electron microscopic morphometric analysis of presence of diaphragms in the capillaries of different organs of $PV1^{-/-}$, $PV1^{ECKO\text{-}Tie}$ and $PV1^{ECRC}$ mice at 4 weeks of age.

		$PV1^{-/-}$		$PV1^{ECKO\text{-}Tie}$		$PV1^{ECRC}$			
Organ	**EC Type**	**Fen/TEC %(stdev)**	**Caveolae %(stdev)**	**Fen/TEC %(stdev)**	**Caveolae %(stdev)**	**Fen/TEC %(stdev)**		**Caveolae %(stdev)**	
							w/FDs		**w/SDs**
Lung	Continuous with SDs	nd	78(6)	nd	88(7)	nd	nd	81(4)	61(12)
Adrenals	Fenestrated	89(5)	76(16)	nd	nd	93(3)	67(4)	95(1.5)	64(7)
Choroid	Fenestrated	96(4)	87(15)	nd	nd	83(14)	64(23)	nd	nd
Kidney PTC	Fenestrated	93(4)	85(3)	95(1)	85(3)	92(4)	77(2)	77(12)	63(4)
Intestine	Fenestrated	81(3)	69(11)	nd	nd	73(12)	45(13)	nd	nd
Pancreas Exo	Fenestrated	91(6)	81(9)	nd	nd	87(4)	59(12)	93(4)	67(8)
Pancreas Endo	Fenestrated	88(1)	77(5)	nd	nd	89(10)	74(3)	78(4)	54(14)
Pituitary	Fenestrated	86(7)	76(3)	nd	nd	93(4)	73(8)	89(13)	47(12)
Salivary gland	Fenestrated	78(9)	65(4)	nd	nd	74(15)	54(17)	64(8)	53(4)
Thyroid	Fenestrated	92(2)	84(1.5)	nd	nd	88(13)	62(14)	79(14)	52(19)
Kidney glomerulus	Fenestrated – no FD	95(2)	nd	94(1)	nd	97(2)	5(4)	nd	nd
Liver sinusoids	Discontinuous – no FD	98(1)	nd	97(2)	nd	98(1)	0	89(4)	69(3)

The data is expressed as the average percentage (+/−stdev) of the fenestrae/TEC and caveolae allowing clear identification of the presence or absence of the diaphragms. Fen/TEC – fenestrae and TEC profiles. nd – not determined.

$watermark-text

$watermark-text

$watermark-text

Table 2

Mouse lines generated to study PV1 function

Name	Genotype	Background	Tissue expression	Survival
PV1$^{-/-}$	PV1$^{L/L}$;CMV-Cre	C57BL/6	All tissues	0% by P2
PV1$^{-/-}$	PV1$^{L/L}$;CMV-Cre	BalbC,BL/6,129	All tissues	20% up to
PV1$^{ECKO-VEC}$	PV1 $^{L/L}$;VEC-Cre	C57BL/6	**EC**, HC	0% by P2
PV1$^{ECKO-VEC}$	PV1 $^{L/L}$;VEC-Cre	BL/6,129	**EC**, HC	20–30% up to 6–7 months
PV1$^{ECKO-Tie2}$	PV1 $^{L/L}$;Tie2-Cre	C57BL/6	**EC**, HC	0% by P2
PV1$^{ECKO-Tie2}$	PV1 $^{L/L}$;Tie2-Cre	BL/6,129	**EC**, HC	20–30% up to 3–4 months
PV1$^{HCKO-Vav}$	PV1 $^{L/L}$;Vav1-Cre	C57BL/6	HC	no phenotype normal life span
PV1$^{HCKO-Vav}$	PV1 $^{L/L}$;Vav1-Cre	BL/6,129	HC	no phenotype normal life span
VEC-PV1HA	VEC-PV1HA	C57BL/6	**EC**	no phenotype normal life span
PV1^{ECRC}	PV1$^{-/-}$;VEC-PV1HA	BalbC, BL/6,129	**EC**	60% up to 18mo